one of these can be neglected without leading to drastic consequences. The implication is that the extent of success of other semiempirical methods, which rely on parameterization, depends on the effectiveness of the parameters to compensate for those quantities which are inherent in the bonding, *i.e.*, neighbor atom potentials, ligand field splittings, environmental charge effects, electron pairing, etc. Although the relative importance of any one, or all of these quantities, is very much a function of the particular environmental influences on the atoms forming the bonds, they must all be integrated to achieve a unified and physically reasonable molecular orbital representation. In methods that are totally computational, this is achieved through the mathematics of the model, but in semiempirical or empirical models these quantities must be explicitly included, which may or may not be possible through the use of arbitrary scaling parameters.

Finally, the success of the present method shows that it is indeed possible to achieve meaningful results through a simplified MO approach without having to resort to the very costly and limited applications of the *ab initio* method. Calculations utilizing the present method are now in progress on other types of systems to provide a further test and will be presented in forthcoming publications.

Registry No. TiF_6^{3-}, 19694-53-2; CrF_6^{3-}, 15276-04-7; FeF_6^{3-}, 17595-31-2; NiF_6^{4-}, 18918-81-5.

Contribution from the Departments of Chemistry and Physics, University of Maine, Orono, Maine 04473

Sharp-Line Luminescence and Absorption for the Hexabromoosmate(IV) Ion in Single Crystals of Cesium Hexabromozirconate(IV) at 20°K

JOHN L. NIMS,[1a] HOWARD H. PATTERSON,*[1a] S. M. KHAN,[1b] and CARMEN M. VALENCIA[1a]

Received December 11, 1972

Strong sharp-line luminescence has been observed for the ($5d^4$) hexabromoosmate(IV) ion in single cubic crystals of the host lattice cesium hexabromozirconate(IV) at 20°K. In the visible and near-infrared regions luminescence is found within the t_{2g}^4 configuration between the $\Gamma_1(^1A_{1g})$ excited state and the four spin-orbit components of the $^3T_{1g}$ ground state. Additional bands are observed in absorption. The major portion of the vibrational structure for each of the band systems is assigned to the ungerade modes of the $OsBr_6^{2-}$ complex in the lattice. The weak vibrational structure may be interpreted in terms of a magnetic dipole mechanism and Jahn–Teller coupling. Good agreement is obtained with available infrared results. The value of the magnetic susceptibility can be calculated from the optical data and is in good agreement with the available susceptibility data for Cs_2OsBr_6.

Introduction

A great amount of luminescence data is available for 3d and 4f transition metal substances. In contrast, little work has been reported in the literature on the luminescence spectra of 4d and 5d transition metal complexes with two exceptions. First, Reinberg and Parker[2,3] have reported the sharp-line luminescence of $ReCl_6^{2-}$ and $OsCl_6^{2-}$ doped in single crystals of Cs_2ZrCl_6 and Cs_2HfCl_6 at 4°K using phase-sensitive detection methods. Second, we have reported recently[4] the sharp-line luminescence and absorption spectra at 20°K for $ReBr_6^{2-}$ doped in Cs_2ZrBr_6. The luminescence reported for the $ReBr_6^{2-}$ ion is sufficiently intense that the absorption and the luminescence were recorded simultaneously on photographic plates without phase-sensitive instrumentation. In this paper we discuss the sharp-line luminescence and absorption spectra for the $5d^4$ system of $OsBr_6^{2-}$ doped as an impurity in the Cs_2ZrBr_6 lattice at 20°K. This system is of interest because selection rules can be derived that describe the nature of vibrational–electronic coupling in d–d type transitions.

Dorain, Patterson, and Jordan[5] have reported the optical absorption spectra for $OsCl_6^{2-}$ doped into Cs_2ZrCl_6, Cs_2HfCl_6, and K_2PtCl_6 at 4°K. Transitions with energies greater than 20,000 cm^{-1} were assigned as of the type $t_{2g}^4 \rightarrow t_{2g}^3 e_g$. Within the t_{2g}^4 configuration the $\Gamma_1(^3T_{1g}) \rightarrow \Gamma_1(^1A_{1g})$ transition was observed at 17,091 cm^{-1}, the $\Gamma_1(^3T_{1g}) \rightarrow \Gamma_5(^1T_{2g})$ transition at 10,733 cm^{-1}, and the $\Gamma_1(^3T_{1g}) \rightarrow \Gamma_3(^1E_g)$ transition at 11,083 cm^{-1}. Also, the energies of the low-lying states arising from the t_{2g}^4 configuration were calculated by means of an intermediate coupling crystal field model. Reinberg[3] has reported luminescence for $OsCl_6^{2-}$ in Cs_2ZrCl_6 at 4°K. Vibronic structure could only be assigned for the $\Gamma_1(^1A_{1g}) \rightarrow \Gamma_1(^3T_{1g})$ transition. Excellent agreement was obtained between the predicted energies of Dorain, Patterson, and Jordan and the Reinberg experimental results for the states arising out of the t_{2g}^4 configuration. Recently, Allen and coworkers[6] have discussed the electronic spectra of OsX_6^{2-} (X = F, Cl, Br, I).

Experimental Section

Cesium hexabromozirconate(IV) was prepared from zirconium tetrabromide (Alfa Inorganics) and cesium bromide (Alfa Inorganics). Stoichiometric amounts of zirconium tetrabromide and cesium bromide were placed in a 9-mm Vycor tube and dried *in vacuo* at 110° for 24 hr. The sealed evacuated Vycor tube was then lowered through a Bridgeman furnace preheated to 800°. The product was allowed to anneal at 500° for 12 hr before the furnace was turned off and the tube was cooled slowly to room temperature. The tube was opened in a drybox and any black impurities were removed with a razor blade. The clearest portions were collected in a new Vycor tube which, after being evacuated and sealed, was passed

(1) (a) Department of Chemistry. (b) Department of Physics.
(2) A. R. Reinberg and S. G. Parker, *Phys. Rev. B*, **1**, 2085 (1970).
(3) A. R. Reinberg, *Phys. Rev. B*, 3, 41 (1971).
(4) H. H. Patterson, J. L. Nims, and C. M. Valencia, *J. Mol. Spectrosc.*, 42, 567 (1972).
(5) P. B. Dorain, H. H. Patterson, and P. C. Jordan, *J. Chem. Phys.*, 49, 3845 (1968).
(6) G. C. Allen, R. Al-Mobarak, G. A. M. El-Sharkawy, and K. D. Warren, *Inorg. Chem.*, 11, 787 (1972).

through the vertical furnace a second time to give optically clear crystals of Cs_2ZrBr_6.

The mixed $Cs_2(Os,Zr)Br_6$ crystals were prepared by placing about 0.5 mol % by weight of Cs_2OsBr_6 with the Cs_2ZrBr_6 in a 9-mm Vycor tube. The tube was evacuated, sealed, and passed through a vertical furnace at a rate of about 2 cm/hr to give optically clear single red crystals. The mixed $Cs_2(Os,Zr)Br_6$ crystals were cleaved with a razor blade to give sections suitable for optical measurements. Several representative samples of the mixed crystals were dissolved in HBr solution and the optical density of the peak at 3970 Å was measured to determine the concentration of Cs_2OsBr_6 in Cs_2ZrBr_6. The amount of the Cs_2OsBr_6 in Cs_2ZrBr_6 was found to be between 0.1 and 0.4 mol %. It has been reported[7] that the d^0 $ZrBr_6^{2-}$ ion does not absorb up to 34,000 cm^{-1}. Also, the amount of luminescence and absorption observed in our studies can be directly correlated with the amount of red color—due to Cs_2OsBr_6—present in the various $Cs_2(Os,Zr)Br_6$ crystal samples. Therefore, the luminescence reported here cannot be due to the host material.

The optical spectrum of the $Cs_2(Os,Zr)Br_6$ single mixed crystals was recorded with a McPherson 1-m Model 2051 monochromator on Kodak 1N and 1M photographic plates. The plate factor was 8.33 Å/mm in the first order. A mercury lamp or a high-pressure xenon lamp was used as the light source. All spectra were calibrated *vs.* an iron-arc spectrum. An Air Products Cryotip (AC3L-110) dewar was used to cool the mounted crystals between room temperature and 20°K. The temperature was measured by means of a chromel-constantan thermocouple.

Results and Discussion

Six electronic transitions each with associated vibrational structure have been observed between 10,000 and 16,500 cm^{-1} for single mixed crystals of $Cs_2(Os,Zr)Br_6$ at 20°K. The first transition shown in Figures 1 and 2 extends in energy from 15,823 to 16,458 cm^{-1} and has both emission and absorption components. The second transition consists of sharp luminescence lines and, as shown in Figures 3-5, is between 12,950 and 13,360 cm^{-1}. The third and fourth transitions are shown in Figure 6. These transitions consist of sharp luminescence lines between 10,821 and 11,119 cm^{-1}. Finally, two transitions are observed only in absorption between 10,000 cm^{-1} and 10,224 cm^{-1}. The line width of these two transitions is between 7 and 26 cm^{-1}; in contrast, the other transitions reported herein have line widths of 5 cm^{-1} or less.

Assignment of Vibrational Structure. To assign the vibrational structure associated with each electronic transition we must consider the possible vibrational states. The normal modes of vibration for the $OsBr_6^{2-}$ complex[8] may be denoted as $\nu_1(a_{1g})$, $\nu_2(e_g)$, $\nu_3(t_{1u})$, $\nu_4(t_{1u})$, $\nu_5(t_{2g})$, and $\nu_6(t_{2u})$ where the expression in parentheses gives the irreducible representation of the octahedral point group according to how the mode transforms. The ν_1, ν_2, and ν_5 modes are Raman active and the ν_4 and ν_3 modes are infrared active. The ν_6 mode is both infrared and Raman inactive.

Brown and co-workers[9] have reported the ν_3 mode of Cs_2OsBr_6 to be 216 cm^{-1}. Woodward and Ware[10] have studied the infrared spectra of Cs_2ReBr_6, Cs_2ReCl_6, and Cs_2OsCl_6 in mulls and the Raman spectra of $ReBr_6^{2-}$, $ReCl_6^{2-}$, and $OsCl_6^{2-}$ in solution. Their measurements indicate the vibrational mode energies of $ReCl_6^{2-}$ and $OsCl_6^{2-}$ complexes are almost identical. It would seem that the vibrational mode energies of $ReBr_6^{2-}$ and $OsBr_6^{2-}$ should also correspond quite closely. Their values for

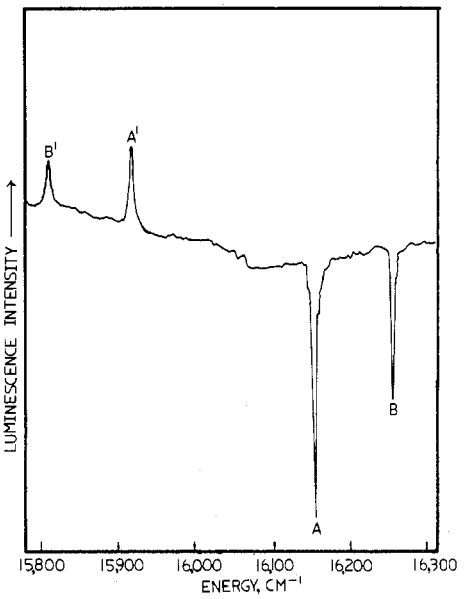

Figure 1. A microphotometer tracing of the optical system $\Gamma_1(^3T_{1g}) \leftrightarrow \Gamma_1(^1A_{1g})$ at 16,039 cm^{-1} for a single mixed $Cs_2(Os,Zr)Br_6$ crystal at 20°K showing both the luminescence and absorption components. The energies and assignments of the peaks are given in Table II.

$ReBr_6^{2-}$ were the following: ν_1 213 cm^{-1}, ν_2 174 cm^{-1}, ν_3 217 cm^{-1}, ν_4 118 cm^{-1}, and ν_5 105 cm^{-1}. From our luminescence experiments[4] on $ReBr_6^{2-}$ doped in Cs_2ZrBr_6 we have found ν_6 to be about 88 cm^{-1}.

For a substance such as Cs_2ZrBr_6 with space group $Fm3m$ Pollack[11] has performed a factor group analysis and showed that at $\vec{k}=0$ there exist three lattice modes of t_{1u}, t_{1g}, and t_{2g} symmetry. The t_{1u} mode, labeled ν_7, is infrared active. Dispersion curves for Cs_2ZrBr_6 have not been determined. However, from the results of Pollack and Satten[12] it is to be expected that the dispersion curves for the internal modes should be relatively flat.

The $OsBr_6^{2-}$ ion doped in the Cs_2ZrBr_6 host lattice possesses inversion site symmetry. Thus a pure electronic d-d electric dipole type transition is parity forbidden. Three mechanisms can account for the appearance of d-d transitions: (1) destruction of inversion symmetry by static distortions; (2) vibrational-electronic coupling to destroy the center of symmetry; (3) magnetic dipole or electric quadrupole mechanism.

For an electronic transition between an initial electronic state i and a final electronic state f to occur the matrix element $\langle \Psi_i^{el} | \underline{O} | \Psi_f^{el} \rangle$ must be nonzero, where $\underline{O}$ is the electric dipole, magnetic dipole, or electric quadrupole operator. For d-d type transitions the initial and final electronic states are gerade. The electric dipole operator transforms as the Γ_{4u} irreducible representation of the O_h point group so no transitions are electric dipole allowed. However, if the ungerade vibrational modes of the final state are considered, we now have $\Gamma_g^{el} \times \Gamma_u^{vib} = \Gamma_u^{vibronic}$. As long as the direct product $\Gamma_i^{el} \times \Gamma\underline{O} \times \Gamma_f^{el} \times \Gamma_u^{vib}$ contains Γ_1 the transition is allowed. For magnetic dipole transitions the operator transforms as Γ_{4g} and zero-zero transitions are allowed. Finally, the irreducible representation for the electric quadrupole operator transforms as Γ_{3g} and Γ_{5g} and so like the magnetic dipole mechanism we might be able to observe

(7) B. J. Brisdon, T. E. Lester, and R. A. Walton, *Spectrochim. Acta, Part A*, 23, 1969 (1967).
(8) F. A. Cotton, "Chemical Applications of Group Theory," Interscience, New York, N. Y., 1963, Chapter 9.
(9) D. H. Brown, K. R. Dixon, C. M. Livingston, R. H. Nuttall, and D. W. A. Sharp, *J. Chem. Soc. A*, 100 (1967).
(10) L. A. Woodward and M. J. Ware, *Spectrochim. Acta*, 20, 711 (1964).
(11) S. A. Pollack, *J. Chem. Phys.*, 38, 98 (1963).
(12) S. A. Pollack and R. A. Satten, *J. Chem. Phys.*, 36, 804 (1962).

Table I. Magnetic Dipole, Electric Quadrupole, and Vibronic Selection Rules for the $OsBr_6^{2-}$ Complex[a]

Symmetry of final electronic state	Symmetry of initial vibrationless electronic state				
	Γ_1	Γ_2	Γ_3	Γ_4	Γ_5
Γ_1			EQ	MD	EQ
	ν_4, ν_3	ν_6	ν_6, ν_4, ν_3	ν_6, ν_4, ν_3	ν_6, ν_4, ν_3
Γ_2			EQ	EQ	MD
	ν_6	ν_4, ν_3	ν_6, ν_4, ν_3	ν_6, ν_4, ν_3	ν_6, ν_4, ν_3
Γ_3	EQ	EQ	EQ	MD, EQ	MD, EQ
	ν_6, ν_4, ν_3	ν_6, ν_4, ν_3	ν_6, ν_4, ν_3	ν_6, ν_4, ν_3	ν_6, ν_4, ν_3
Γ_4	MD	EQ	MD, EQ	MD, EQ	MD, EQ
	ν_6, ν_4, ν_3	ν_6, ν_4, ν_3	ν_6, ν_4, ν_3	ν_6, ν_4, ν_3	ν_6, ν_4, ν_3
Γ_5	EQ	MD	MD, EQ	MD, EQ	MD, EQ
	ν_6, ν_4, ν_3	ν_6, ν_4, ν_3	ν_6, ν_4, ν_3	ν_6, ν_4, ν_3	ν_6, ν_4, ν_3

[a] The notation MD or EQ means the transition is magnetic dipole allowed or electric quadrupole allowed, respectively. Also, the symmetry of vibrations allowing d-d transitions is given.

Table II. Energies and Assignments for the Luminescence and Absorption Spectrum of Single Mixed $Cs_2(Os,Zr)Br_6$ Crystals at 20°K in the 10,821–16,254-cm^{-1} Energy Region

Figure No.	Peak	Obsd energy, cm^{-1}	Assignment
1	B′	15,822.7	$\Gamma_1(^1A_{1g}) \rightarrow \Gamma_1(^3T_{1g}) + \nu_3$
	A′	15,924.2	$\Gamma_1(^1A_{1g}) \rightarrow \Gamma_1(^3T_{1g}) + \nu_4$
	A	16,157.1	$\Gamma_1(^3T_{1g}) \rightarrow \Gamma_1(^1A_{1g}) + \nu_4$
	B	16,253.8	$\Gamma_1(^3T_{1g}) \rightarrow \Gamma_1(^1A_{1g}) + \nu_3$
2	1	16,067.6	$\Gamma_1(^3T_{1g}) \rightarrow \Gamma_1(^1A_{1g})$ + lm[a]
	2	16,083.8	+ lm
	3	16,107.7	+ lm
	A	16,157.1	+ ν_4
	B	16,253.8	+ ν_3
	C	16,363.9	+ $(\nu_4 + \nu_1)$
	D	16,458.4	+ $(\nu_3 + \nu_1)$
3	0′	13,280.1	$\Gamma_1(^1A_{1g}) \rightarrow \Gamma_4(^3T_{1g})$
	A′	13,194.3	+ ν_6
	B′	13,162.9	+ ν_4
	C′	13,062.7	+ ν_3
4	A²	13,359.9	$\Gamma_1(^1A_{1g}) + \nu_6 \rightarrow \Gamma_4(^3T_{1g})$
	0′	13,280.1	$\Gamma_1(^1A_{1g}) \rightarrow \Gamma_4(^3T_{1g})$
	1	13,252.9	+ lm
	2	13,236.9	+ lm
	3	13,221.1	+ lm
	A′	13,194.3	+ ν_6
	B′	13,162.9	+ ν_4
		13,133.2	
	G′	13,102.0	+ ν_2
	H′	13,079.2	
	C′	13,062.7	+ ν_3
5	D′	13,012.2	$\Gamma_1(^1A_{1g}) \rightarrow \Gamma_4(^3T_{1g}) + (\nu_2 + \nu_6)$
	E′	12,979.5	+ $(\nu_1 + \nu_6)$
	F′	12,950.3	+ $(\nu_1 + \nu_4)$
6	A′	11,119	$\Gamma_1(^1A_{1g}) \rightarrow \Gamma_5(^3T_{1g}) + \nu_4$
	B′	11,027	$\Gamma_5(^3T_{1g}) + \nu_3$
	C′	11,017	
	D′	10,986	$\Gamma_3(^3T_{1g}) + \nu_6$
	E′	10,956	$\Gamma_3(^3T_{1g}) + \nu_4$
	F′	10,924	$\Gamma_5(^3T_{1g}) + (\nu_4 + \nu_1)$
	G′	10,857	$\Gamma_3(^3T_{1g}) + \nu_3$
	H′	10,821	$\Gamma_5(^3T_{1g}) + (\nu_3 + \nu_1)$

[a] Abbreviation lm means lattice mode.

0-0 transitions. Selection rules are given in Table I. The predicted transition probabilities are in the order[13] of electric dipole allowed ≫ magnetic dipole allowed ≫ electric quadrupole allowed. The assignment of the vibrational structure for the individual transitions will now be discussed. The observed or calculated origin for each electronic transition will be used as an index for the spectrum of a given electronic transition. The energies and assignments of the various peaks are given in Tables II and III. The electronic assignments will be discussed in another section of this paper.

(13) J. S. Griffith, "The Theory of Transition-Metal Ions," Cambridge University Press, New York, N. Y., 1961, Chapter 11.

Table III. Energies and Assignments for the Absorption Spectrum in the 10,000–10,224-cm^{-1} Region for $Cs_2(Os,Zr)Br_6$ Crystals at 20°K

Peak (of Figure 7)	Obsd energy, cm^{-1}	Assignment
A	10,000	$\Gamma_1(^3T_{1g}) \rightarrow \Gamma_5(^1T_{2g}) + \nu_6$
B	10,031	$\rightarrow \Gamma_5(^1T_{2g}) + \nu_4$
C	10,052	$\rightarrow \Gamma_3(^1E_g) + \nu_6$
D	10,086	$\rightarrow \Gamma_3(^1E_g) + \nu_4$
E	10,102	
F	10,128	$\rightarrow \Gamma_5(^1T_{2g}) + \nu_3$
G	10,184	$\rightarrow \Gamma_3(^1E_g) + \nu_3$
H	10,196	$\rightarrow \Gamma_5(^1T_{2g}) + (\nu_3 + \nu_1)$
1	10,224	$\rightarrow \Gamma_5(^1T_{2g}) + (\nu_4 + \nu_1)$

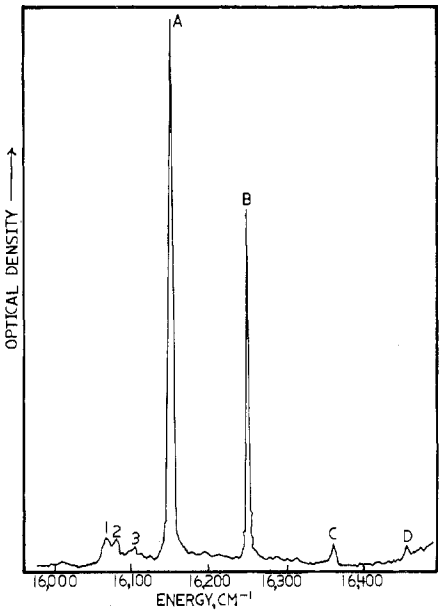

Figure 2. A microphotometer tracing of a photographic plate showing the optical absorption spectrum for the $\Gamma_1(^3T_{1g}) \rightarrow \Gamma_1(^1A_{1g})$ transition given in Figure 1 with increased vibronic detail.

$\Delta E = 16{,}039\ cm^{-1}$, $\Gamma_1(^3T_{1g}) \leftrightarrow \Gamma_1(^1A_{1g})$. For the spectrum shown in Figure 1 the emission and absorption portions form symmetrical mirror images of each other. The energy difference between emission peaks B′ and A′ is 101.5 cm^{-1} while the energy difference between absorption peaks B and A is 96.3 cm^{-1}. These energy differences correspond closely to the ν_3-ν_4 energy separation. Thus, peaks A′ and B′ are assigned to ν_4 and ν_3 of the ground electronic state while A and B are assigned to ν_4 and ν_3 of the excited electronic state. If the system is assigned as $\Gamma_1(^3T_{1g}) \leftrightarrow \Gamma_1(^1A_{1g})$ we see from the selection rules in Table I that only the ν_4 and ν_3 modes should appear (not the ν_6 mode) and the 0-0 no-phonon transition is forbidden. This is in complete agreement with our experimental results.

Figure 2 gives in greater detail the absorption portion of the $\Gamma_1(^1A_{1g}) \leftrightarrow \Gamma_1(^3T_{1g})$ system. The energy difference between peaks A and C is 207 cm^{-1}, and that between B and D is 205 cm^{-1}, so we assign peak C as $\nu_4 + \nu_1$ and peak D as $\nu_3 + \nu_1$. If we use the Brown, *et al.*, value[9] of 216 cm^{-1} for the ν_3 mode of the ground electronic state, we calculate the origin of the transition to be at 16,039 cm^{-1}. This gives energy values for peaks 1, 2, and 3 of 29, 45, and 59 cm^{-1}, respectively. These peaks may be assigned as lattice

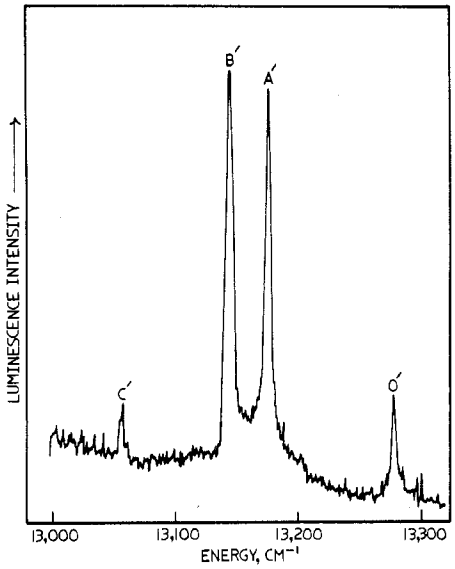

Figure 3. A microphotometer tracing of the luminescence spectrum of the $\Gamma_1(^1A_{1g}) \rightarrow \Gamma_4(^3T_{1g})$ transition at 13,280 cm^{-1}. The lines are labeled according to Table II.

modes and should be compared with the lattice mode energies for $Cs_2(Re,Zr)Br_6$ of 30, 40, and 63 cm^{-1}.

It should be pointed out that on the basis of the lattice selection rules derived by Pollack[11] for the case where the wave vector $\vec{k} = 0$ only one lattice mode should appear in the Figure 2 spectrum. The fact that three lattice modes are present indicates that points of high symmetry in the Cs_2ZrBr_6 Brillouin zone other than $\vec{k} = 0$ must be considered where there is a corresponding high density of phonon states within a narrow energy range. Unfortunately, no lattice dynamics calculations have been performed for the host lattice; therefore, we will not be able to give specific assignments for the three lattice peaks except to say that consideration of selection rules at the special symmetry points X and L in the Brillouin zone for Cs_2ZrBr_6 will indicate probable lattice mode assignments. We choose not to pursue this discussion any further at this time. The interested reader is referred to the papers by Loudon[14] and by O'Leary and Wheeler.[15]

$\Delta E = 13{,}280.1\ cm^{-1}$, $\Gamma_1(^1A_{1g}) \rightarrow \Gamma_4(^3T_{1g})$. Figure 3 shows the emission spectrum observed at about 13,280 cm^{-1}. The peak energies and assignments are given in Table II. The four peaks may be assigned easily. The energy differences between 0′ and A′, B′, and C′ are 85.8, 117.2, and 217.4 cm^{-1}. Since these differences nearly correspond to the ν_6, ν_4, and ν_3 vibrational mode energies reported by Woodward and Ware for $ReBr_6^{2-}$, we assign line 0′ as the 0-0 transition and lines A′, B′, and C′ to the ν_6, ν_4, and ν_3 modes of the final electronic state.

In Figures 4 and 5 microphotometer tracings are given of photographic plates with long time exposures to show the fine detail present in the 13,280-cm^{-1} luminescence spectrum. The peak A^2 is 82 cm^{-1} greater in energy than 0′ and is assigned to ν_6 of the initial electronic state. Peaks E′ and F′ are assigned as $(\nu_6 + \nu_1)$ and $(\nu_4 + \nu_1)$ for the final electronic state, respectively, with the value of ν_1 equal to 214 cm^{-1}. Three weak lines, assigned to lattice modes, have been observed with energies of 28.2, 43.2, and 59.0 cm^{-1}.

Peaks G′ and D′ can be assigned to ν_2 and $(\nu_2 + \nu_6)$, respectively, of the final electronic state, with the value of ν_2 equal to 178 cm^{-1}. If the electronic transition is $\Gamma_1 \rightarrow \Gamma_4$, with the final electronic state threefold degenerate, it is possible to interpret the appearance of the $\nu_2(e_g)$ mode as evidence for weak dynamic Jahn-Teller coupling being present in the Γ_4 electronic state. Brand, Goodman, and Weinstock[16,17] have measured the optical absorption spectrum of ReF_6 and IrF_6. Short progressions were found to be present not only in the ν_1 mode but also in the ν_2 and ν_5 modes. From an analysis of the intensity distribution in the progressions it was possible to calculate the magnitude of the weak dynamic Jahn-Teller coupling. Work is under way in our laboratory to perform a similar analysis for the $OsBr_6^{2-}$ case.

$\Delta E = 11{,}073\ cm^{-1}$, $\Gamma_1(^1A_{1g}) \rightarrow \Gamma_3(^3T_{1g})$; $\Delta E = 11{,}236\ cm^{-1}$, $\Gamma_1(^1A_{1g}) \rightarrow \Gamma_5(^3T_{1g})$. In Figure 6 a microphotometer

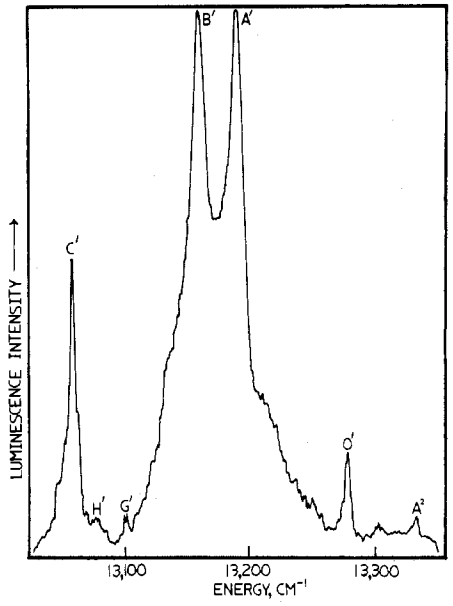

Figure 4. A microphotometer tracing of the $\Gamma_1(^1A_{1g}) \rightarrow \Gamma_4(^3T_{1g})$ transition given in Figure 3 showing increased vibrational detail.

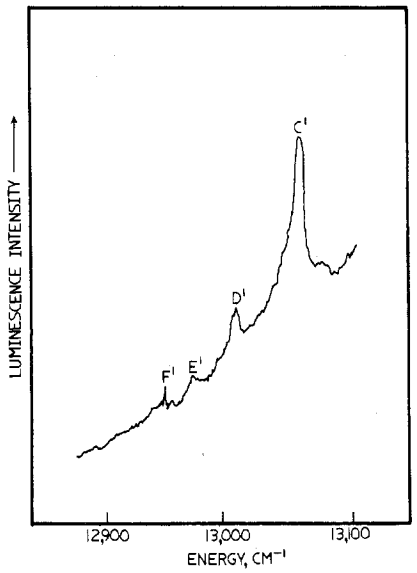

Figure 5. A microphotometer tracing of a photographic plate showing the tail of the luminescence spectrum for the $\Gamma_1(^1A_{1g}) \rightarrow \Gamma_4(^3T_{1g})$ spectrum.

(14) R. Loudon, *Proc. Phys. Soc., London*, 84, 379 (1964).
(15) G. P. O'Leary and R. G. Wheeler, *Phys. Rev. B*, 1, 4409 (1970).
(16) J. C. D. Brand, G. L. Goodman, and B. Weinstock, *J. Mol. Spectrosc.*, 38, 449 (1971).
(17) J. C. D. Brand, G. L. Goodman, and B. Weinstock, *J. Mol. Spectrosc.*, 37, 464 (1971).

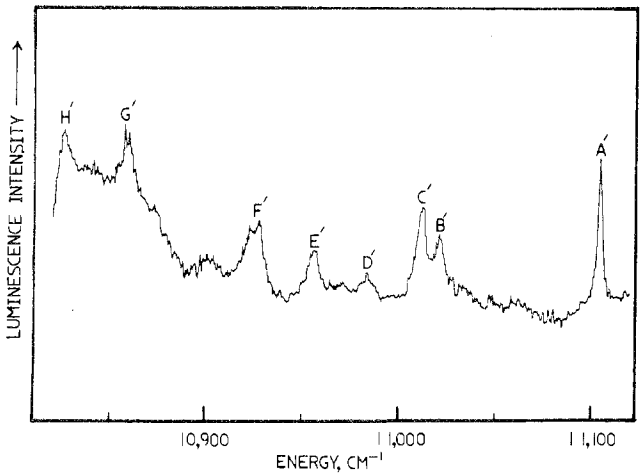

Figure 6. A microphotometer tracing showing the $\Gamma_1(^1A_{1g}) \rightarrow \Gamma_3(^3T_{1g})$, $\Gamma_5(^3T_{1g})$ luminescence spectrum at about 11,000 cm^{-1}. The energies and assignments of the various peaks are given in Table II.

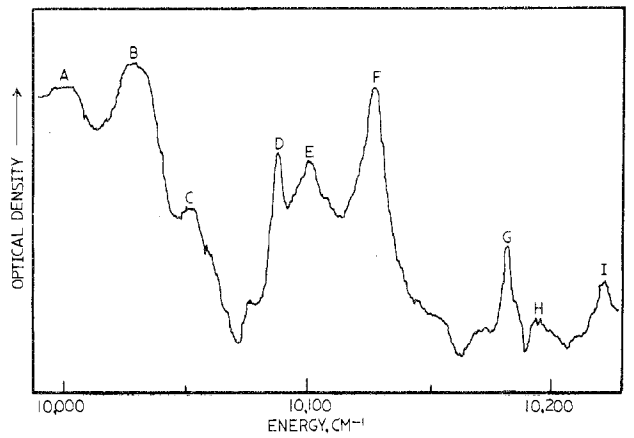

Figure 7. A microphotometer tracing showing the absorption spectrum at about 10,000 cm^{-1} assigned to a transition between the $\Gamma_1(^3T_{1g})$ ground state and the $\Gamma_3(^1E_g)$, $\Gamma_5(^1T_{2g})$ excited states. The peaks are labeled according to Table III.

tracing is shown of the luminescence spectrum recorded between 10,821 and 11,119 cm^{-1}. The quality of the tracing is somewhat less than the preceding tracings due to the use of M photographic plates in this region. The spectrum is assigned as a transition between an initial vibrationless electronic state and two final electronic states. It has not been possible to assign the spectrum to one final electronic state alone. Peaks A' and C'-B' are assigned to ν_4 and ν_3 of one final electronic state. Further, peaks D', E', and G' are assigned to ν_6, ν_4, and ν_3, respectively, of a second final electronic state. If we assume ν_4 to be 117 cm^{-1} for both final electronic states, a value of 11,236 cm^{-1} is obtained for the origin of the first transition and a value of 11,073 cm^{-1} for the origin of the second transition.

$\Delta E = 9914\ cm^{-1}$, $\Gamma_1(^3T_{1g}) \rightarrow \Gamma_5(^1T_{2g})$; $\Delta E = 9969\ cm^{-1}$, $\Gamma_1(^3T_{1g}) \rightarrow \Gamma_3(^1E_g)$. Figure 7 shows a copy of a microphotometer tracing of the absorption spectrum recorded between 10,000 and 10,224 cm^{-1}. In this spectral region M photographic plates were used. The energies and assignments of the various peaks are given in Table III. Peaks A, B, and F are assigned as ν_6, ν_4, and ν_3, respectively, to one final electronic state. Peaks C, D, and G are assigned in a similar fashion to ν_6, ν_4, and ν_3, respectively, of a second final electronic state. If we assume ν_4 of both final electronic states to be 117 cm^{-1}, a value of 9914 cm^{-1} is obtained for the origin of the first transition while a value of 9969 cm^{-1} is obtained for the origin of the second transition.

Electronic Assignments. Osmium(4+) has a d^4 electronic configuration. When the ion is placed in an octahedral crystal field the following terms result within the t_{2g}^4 configuration in order of increasing energy: $^3T_{1g}$, $^1T_{2g}$, ^1E_g, $^1A_{1g}$. These terms will be split by spin-orbit interaction into states which can be denoted in the Bethe notation as Γ_i ($i = 1$-5) where Γ_i is the appropriate irreducible representation of the cubic group. Magnetic susceptibility measurements[18] indicate that the spin-orbit interaction is of the same order of magnitude as the interelectronic repulsion and cannot be treated simply by perturbation theory alone.

It is possible to estimate the approximate energies of the various electronic t_{2g}^4 states by use of the p^n isomorphism to t_{2g}^{6-n}, discussed by Moffitt, Goodman, Fred, and Weinstock.[19] Moffitt and coworkers found that the states arising from the t_{2g}^n configuration in octahedral symmetry are formally identical with those of the atomic configuration p^{6-n}. As a result of this equivalence the magnitude of the interelectronic repulsive interaction may now be assessed by a single parameter ($3B + C$), whose magnitude relative to that of the spin-orbit parameter ξ determines the coupling scheme (Russell-Saunders, intermediate coupling, or j-j). In terms of the ratio of the interelectronic repulsion to the spin-orbit interaction one can calculate an energy level diagram for the states arising out of the t_{2g}^4 configuration. Moffitt, *et al.*, have done this for the d^4 system PtF_6. In Figure 8 we show such a diagram. Comparing the absorption spectrum of PtF_6 with the energy level diagram, Moffitt, *et al.*, concluded that a satisfactory assignment of the weak-band systems could be made on the basis of transitions within the t_{2g}^4 configuration for $\xi = 3400\ cm^{-1}$, $3B + C = 2400\ cm^{-1}$, and the ratio of $\xi/(3B + C) = 1.4$. Similar success was attained in analyzing the weak-band systems in ReF_6, OsF_6, and IrF_6 with $\xi/(3B + C) = 1.4$.

In the first step of our analysis it was assumed that the t_{2g}^4 states in $OsBr_6^{2-}$ are at about the same energy as with PtF_6. The system observed at 16,039 cm^{-1} in both absorption and emission is then assigned as $\Gamma_1(^3T_{1g}) \leftrightarrow \Gamma_1(^1A_{1g})$ in contrast to 16,000 cm^{-1} reported for PtF_6. Second, the luminescence spectrum with origin at 13,280 cm^{-1} is assigned as a transition from the $\Gamma_1(^1A_{1g})$ state to the Γ_4 component of the spin-orbit split $^3T_{1g}$ ground state; therefore, the $\Gamma_4(^3T_{1g})$ state is 2759 cm^{-1} above the ground state in $OsBr_6^{2-}$ in contrast to the value of 3300 cm^{-1} for PtF_6. Next, the two absorption spectra observed at about 9942 cm^{-1} are assigned as $\Gamma_1(^3T_{1g}) \rightarrow \Gamma_5(^1T_{2g})$, $\Gamma_3(^1E_g)$ in contrast to the 12,000-cm^{-1} value for PtF_6. It should be noted that the two excited states $\Gamma_5(^1T_{2g})$ and $\Gamma_3(^1E_g)$ are degenerate in the p^n-t_{2g}^{6-n} approximation; however, when configuration interaction is included,[5] they become somewhat separated with the $\Gamma_3(^1E_g)$ state lying higher in energy than the $\Gamma_5(^1T_{2g})$ state. Finally, it should follow that the two transitions observed in luminescence at about 11,155 cm^{-1} correspond to the transitions $\Gamma_1(^1A_{1g}) \rightarrow \Gamma_3(^3T_{1g})$, $\Gamma_5(^3T_{1g})$ with the Γ_5, Γ_3 states calculated to be at 4887 cm^{-1} in contrast to 5500 cm^{-1} for PtF_6.

In the second step of the analysis a computer program was written to calculate the energies of the t_{2g}^4 states as a function of the parameters ($3B + C$) and ξ. The relevant interelectronic repulsive and spin-orbit matrix elements

(18) A. Earnshaw, B. N. Figgis, J. Lewis, and R. D. Peacock, *J. Chem. Soc.* 3132 (1961).
(19) W. Moffitt, G. L. Goodman, M. Fred, and B. Weinstock, *Mol. Phys.*, 2, 109 (1959).

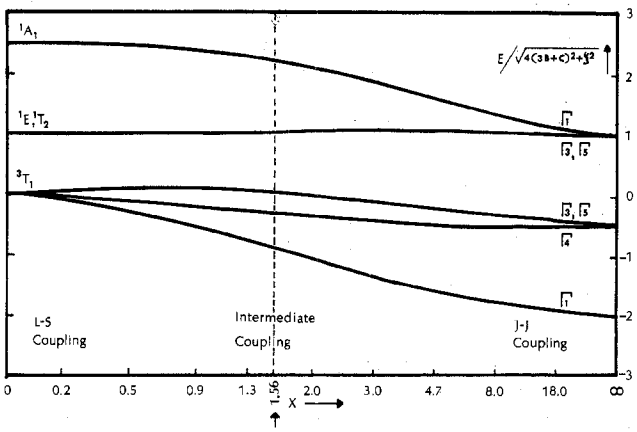

Figure 8. Behavior of the t_{2g}^4 configuration states as a function of the dimensionless parameter $X = \xi/(3B + C)$.

are given by Griffith.[20] For each choice of the parameters $(3B + C)$ and ξ the computer output consisted of the electronic state energies and the root-mean-square (rms) deviation of the calculated energies from the observed energies. The minimum rms deviation was achieved for the choice of parameters $\xi/(3B + C) = 1.561$, $3B + C = 2032$ cm^{-1}, and $\xi = 3172$ cm^{-1}. The rms value was 95 cm^{-1}. Energy level diagrams are given in Figures 9 and 10.

The vibrational analysis presented in the previous section is of some relevance in confirming our assignments. For the $\Gamma_1(^3T_{1g}) \leftrightarrow \Gamma_1(^1A_{1g})$ system the selection rules in Table I predict that a 0-0 no-phonon line should not appear in the spectrum in agreement with experiment and that the $\nu_6(t_{2u})$ mode should not appear, again in agreement with experiment. Next, for the $\Gamma_1(^1A_{1g}) \rightarrow \Gamma_4(^3T_{1g})$ transition the magnetic dipole selection rules predict a 0-0 line and the vibronic selection rules predict the appearance of $\nu_6(t_{2u})$, $\nu_4(t_{1u})$, and $\nu_3(t_{1u})$ modes, all in agreement with our data. The other transitions observed have vibrational mode assignments in agreement with the selection rules in Table I.

It should be pointed out that at energies greater than 17,500 cm^{-1} a number of strong absorptions occur for the $OsBr_6^{2-}$ complex. Schatz and coworkers[21] in a recent study have assigned these transitions as charge transfer in nature from their low-temperature high-resolution magnetic circular dichroism and absorption studies. Dorain, Patterson, and Jordan[5] in a low-temperature absorption study of $OsCl_6^{2-}$ assigned these transitions as of the type $t_{2g}^4 \rightarrow t_{2g}^3 e_g$. In this paper we choose not to discuss these higher energy transitions except to point out that the closeness of these states to the t_{2g}^4 states will result in configuration interaction mixing these states with the t_{2g}^4 states in an unknown way.

Magnetic Susceptibility. In 1954 Johannesen and Lindberg[22] reported for ammonium hexabromoosmate a temperature-independent molar magnetic susceptibility of $(980 \pm 20) \times 10^{-6}$ cm^3 mol^{-1} in the temperature range of 100-400°K. In 1961 Westland and Bhiwandker[23] reported measurements on solid solutions of K_2OsCl_6 and K_2OsBr_6 diluted with diamagnetic K_2PtCl_6 and K_2PtBr_6, respectively,

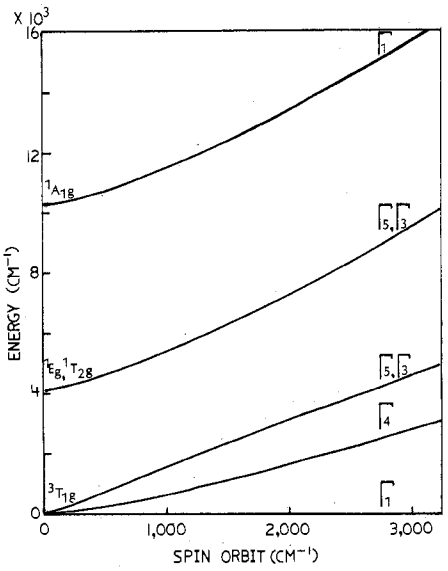

Figure 9. Energy level diagram for the t_{2g}^4 states of a d^4 ion in a strong octahedral field. Energies are plotted as a function of increasing spin-orbit interaction. The value of 2032 cm^{-1} has been used for the Coulomb interaction parameter, $3B + C$.

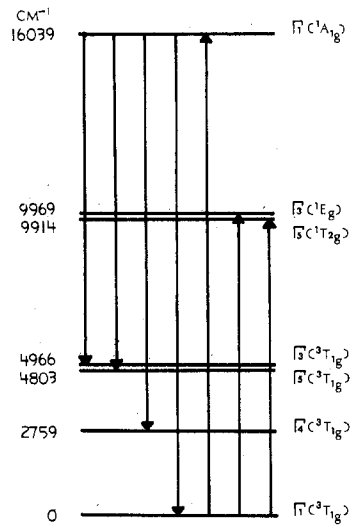

Figure 10. Energy level diagram for the $OsBr_6^{2-}$ complex at 20°K showing the observed electronic transitions.

which showed that the paramagnetism of the osmium salts increased with dilution. They proposed that extensive superexchange takes place through the overlap of d orbitals on the osmium atom and orbitals on the ligands in the pure substances and in the concentrated crystals.

Johannesen and Candela[24] in 1962 reported magnetic susceptibility measurements on a series of hexachloro- and hexabromoosmates, with the paramagnetism independent of temperature between 78 and 278°K. $(NH_4)_2OsBr_6$ had a molar magnetic susceptibility of 991×10^{-6} cm^3 mol^{-1} and Cs_2OsBr_6 has a molar magnetic susceptibility of 988×10^{-6}. They found that the paramagnetism of the Os(IV) complexes increases as the osmium ions are separated and that the effect of dilution can be described by the equation $\chi = \chi_\infty/(1 + \lambda d^{-n}\chi_\infty)$ where χ_∞ is the susceptibility at infinite dilution, d is the average distance between the osmium ions, λ is a constant, and n is approximately 2. The susceptibility was found to be neither strongly affected by the

(20) J. S. Griffith, "The Theory of Transition-Metal Ions," Cambridge University Press, New York, N. Y., 1961, p 282.
(21) W. H. Inskeep, R. W. Schwartz, and P. N. Schatz, *Mol. Phys.*, in press.
(22) R. B. Johannesen and A. R. Lindberg, *J. Amer. Chem. Soc.*, 76, 5349 (1954).
(23) A. D. Westland and N. C. Bhiwandker, *Can. J. Chem.*, 39, 1284 (1961).
(24) R. B. Johannesen and G. A. Candela, *Inorg. Chem.*, 2, 67 (1963).

nature of the cations nor by the type of halogen ligand. The fact that the halogen ligand does not have a great effect on the susceptibility would indicate that superexchange *via* the halogen atom cannot be very important in determining the amount of exchange. Greenslade[25] has suggested that ligand fields of lower than cubic symmetry can explain the dilution effects.

To compare the magnetic susceptibility measurements with the optical analysis we can make use of the low-spin d^4 model of Griffith.[20] The ground state transforms as the Γ_1 irreducible representation and is nonmagnetic; also, the energy difference between the ground state and the low-lying Γ_4 excited state is great enough so that only the ground state will be appreciably populated in the temperature range of the magnetic measurements. Van Vleck paramagnetism arises from the admixture by an applied magnetic field of excited Γ_4 magnetic states with the ground state resulting in a measured magnetic susceptibility independent of temperature. Griffith used the isomorphism between the t_{2g}^4 and p^2 configurations to derive an expression for the susceptibility of low-spin d^4 complexes. He gave

$$\chi_M = \frac{2N\beta^2(1 + \cos\theta)(k + 2)^2}{3\delta(\sqrt{2}/4 \tan\theta - 1 + \sec\theta)}$$

where $\delta = {}^1/_2(15B + 5C + \xi)k$, $\tan\theta = \sqrt{2}\xi/\theta$, and k is the orbital reduction factor. The contribution to the susceptibility from the higher configuration states was estimated by Griffith to be about $(50\text{-}70) \times 10^{-6}$ cm^3 mol^{-1}.

If the values of $(3B + C)$ and ξ calculated from the crystal field analysis of the optical data are substituted into the Griffith expression, with the orbital reduction factor equal to 1, the value of χ_M calculated for Cs_2OsBr_6 is 947×10^{-6} cm^3 mol^{-1}. The value of χ_M measured for pure Cs_2OsBr_6 is 988×10^{-6} cm^3 mol^{-1} by Johannesen and Candela. This represents less than a 5% difference between the value of χ_M calculated from the optical data for the dilute case, Cs_2OsBr_6 in Cs_2ZrBr_6, and the χ_M measured for pure Cs_2OsBr_6. When only the $\Gamma_4(^3T_{1g})$ excited state and the $\Gamma_1(^1A_{1g})$ excited state are fit to the crystal field model and the other states are ignored, the χ_M calculated becomes 1022 cm^3 mol^{-1} with an rms deviation between the observed energies and calculated energies of 1.2 cm^{-1}. In this case the difference between the calculated and measured χ_M values is about 4%.

Griffiths and Owens[26] have estimated the orbital reduction factor to be 0.84 for K_2IrCl_6 and K_2IrBr_6 from analysis of the hyperfine structure in the electron paramagnetic resonance spectrum. No data are available for the osmium(4+) salts. If k becomes 0.84, χ_M decreases by 90×10^{-6} cm^3 mol^{-1}. Also, Dorain, Patterson, and Jordan[5] in their analysis of K_2OsCl_6 have shown that the states arising from the $t_{2g}^3e_g$ configuration contribute about $+100 \times 10^{-6}$ cm^3 mol^{-1} to the susceptibility and this contribution has not been included in the Griffith formula. Thus, it would seem that inclusion of the orbital reduction effect is about balanced out by the $t_{2g}^3e_g$ states contribution to the susceptibility, and the calculation of χ_M from the Griffith formula is a reasonable approach.

The fact that the susceptibilities for the pure Cs_2OsBr_6 system and for the dilute undistorted Cs_2OsBr_6-Cs_2ZrBr_6 system are in good agreement would suggest that the Westland-Bhiwandker dilution effects can be explained by distortion effects present in the K_2OsBr_6-K_2PtBr_6 system. In an effort to prove this we have grown single K_2OsBr_6-K_2PtBr_6 mixed crystals with a molar concentration for K_2OsBr_6 of about 1 mol %. Initial optical experiments in our laboratory at 20°K show that the $\Gamma_1(^3T_{1g}) \rightarrow \Gamma_1(^1A_{1g})$ spectrum for K_2OsBr_6 in K_2PtBr_6 is very broad and shifted from the spectrum in Figure 1 for Cs_2OsBr_6 in Cs_2ZrBr_6. Further details of this study will be published at a later date.

Registry No. Cesium hexabromozirconate(IV), 36407-58-6; Cs_2OsBr_6, 19121-80-3.

Acknowledgments. This research has been supported in part by a Frederick Gardner Cottrell Grant from the Research Corp. and in part by a grant from the Faculty Research Fund of the University of Maine at Orono. The computations reported herein were performed at the University of Maine Computation Center. We wish to thank Dr. Paul N. Schatz and Dr. Paul Dorain for many helpful discussions and, finally, Dr. P. L. Goodfriend for his interest and encouragement in these studies.

(25) D. J. Greenslade, *J. Chem. Soc. A*, 834 (1968).

(26) See A. Abragam and B. Bleaney "Electron Paramagnetic Resonance of Transition Ions," Clarendon Press, Oxford, 1970, pp 480-484.